Supplementary Information for

Effects of polymer network flexibility on the kinetics of DEZ vapor phase infiltration into photo-polymerized polyacrylates

Lisanne Demelius[a,b], Anna Maria Coclite[a] and Mark D. Losego[b]

[a] Institute of Solid State Physics, Graz University of Technology, Graz, Austria.
[b] School of Materials Science and Engineering, Georgia Institute of Technology, Atlanta, GA, USA

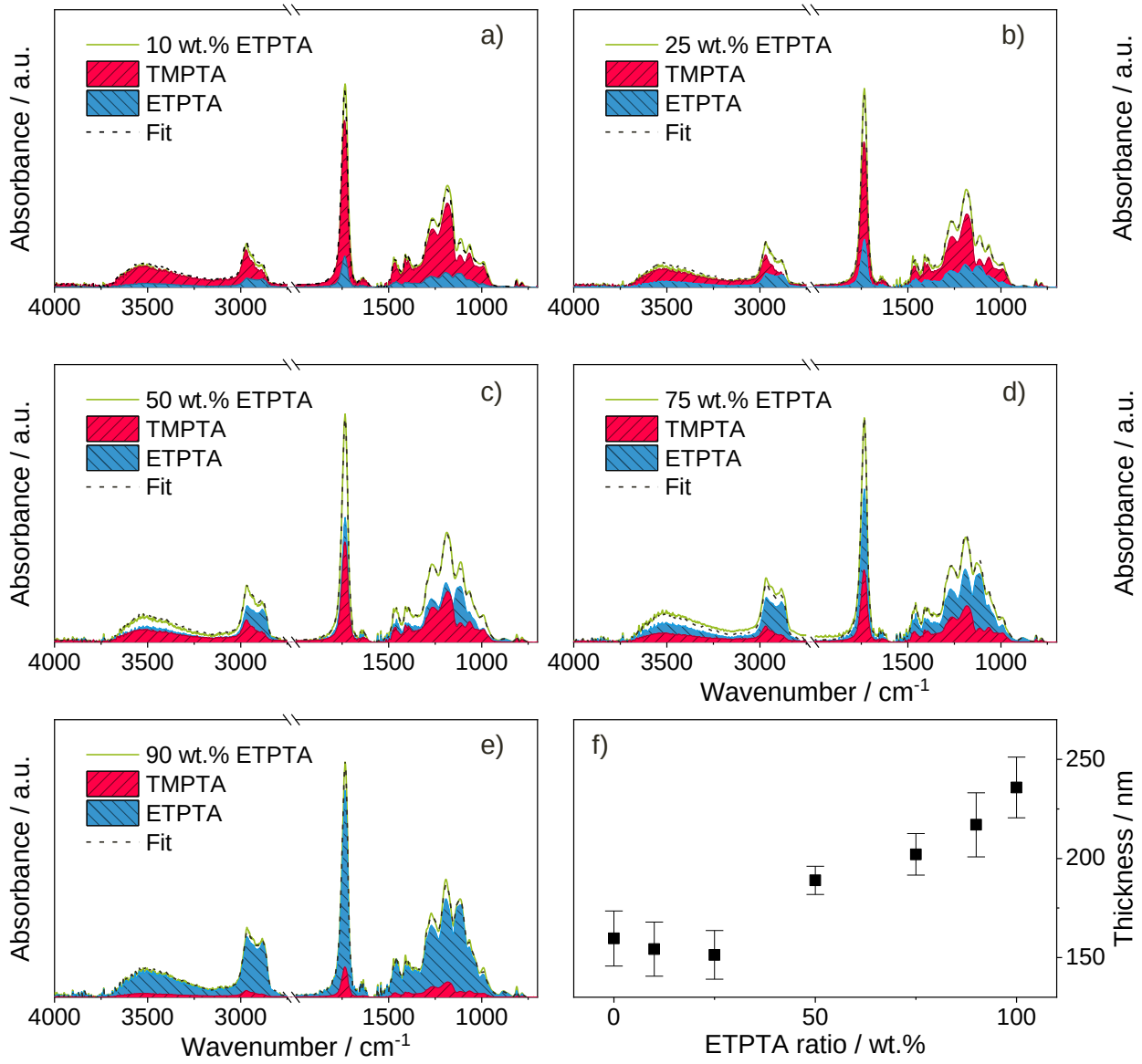

Figure S1: a)-e) Fitted FTIR absorbance spectra for different monomer mixing ratios of a)10, b) 25, c) 50, d) 75 and e) 90 wt.% ETPTA. f) Average copolymer film thickness measured by ellipsometry as a function of ETPTA weight ratio. The thickness values have been averaged over 6-12 samples for each composition.

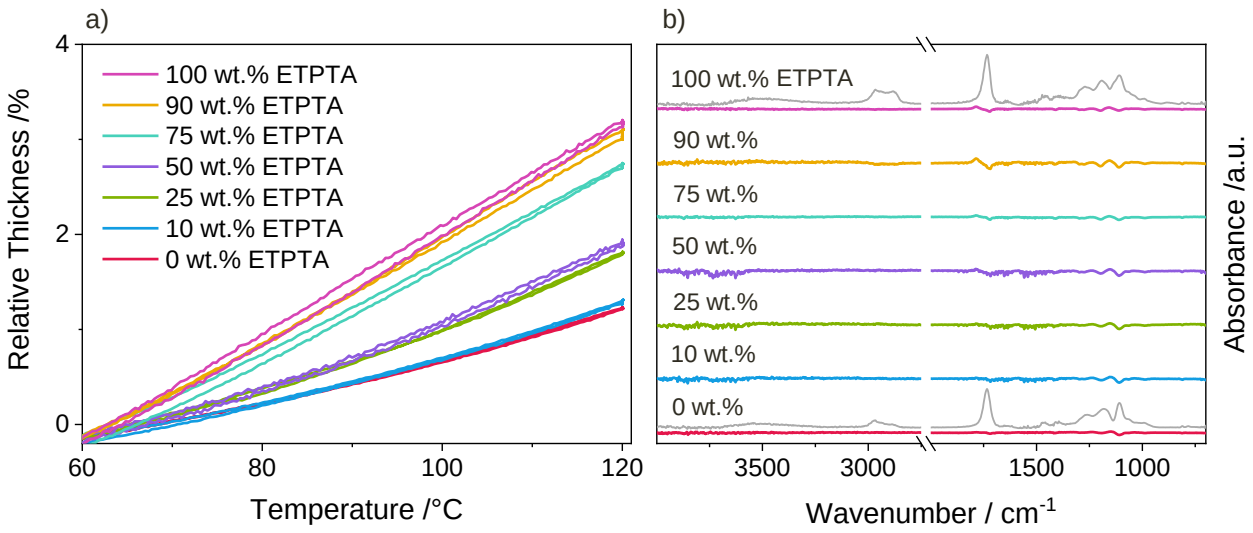

Figure S2: a) Thermal expansion of p(TMTPA-ETPTA) copolymer thin films of different compositions measured by ellipsometry. The linear thermal expansion coefficient displayed in **Figure 2** was calculated by linear fitting in the temperature range from 80-120 ° C. b) FTIR difference spectra of copolymer films of different compositions after heating to 120 ° C for 24 h under vacuum. For the two homopolymers, the absolute FTIR absorbance spectra before heat exposure is displayed in gray.

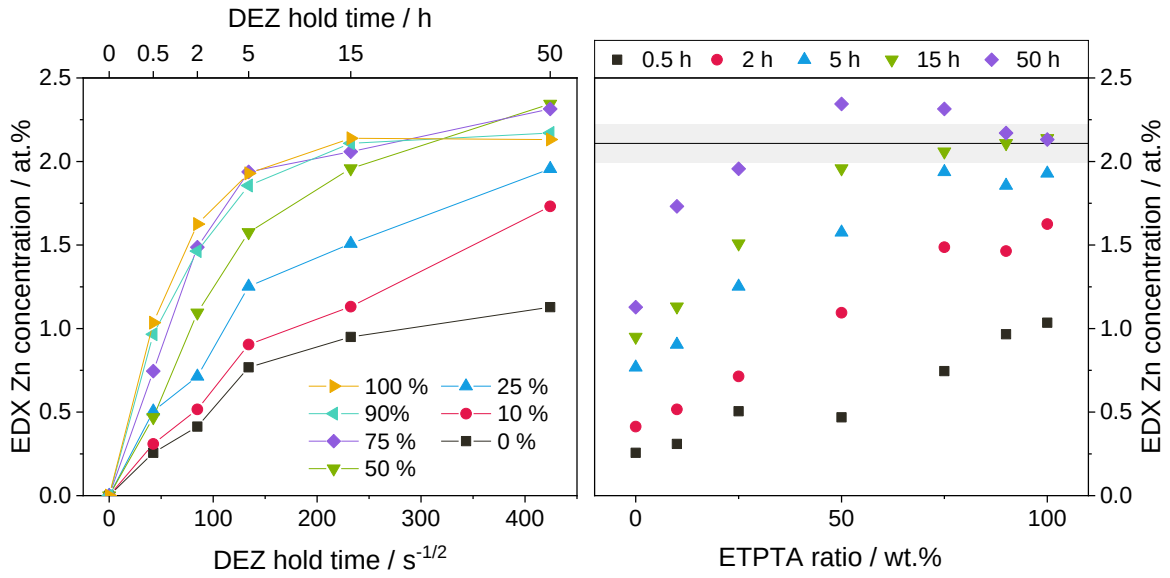

Figure S3: Zn loading of p(TMPTA-ETPTA) films after VPI at 120 ° C as a function of a) ETPTA ratio in the copolymer and b) DEZ hold time determined by the fitted EDX atomic Zn concentration. In b), the horizontal line and the gray area indicate the average saturation loading and its standard deviation.

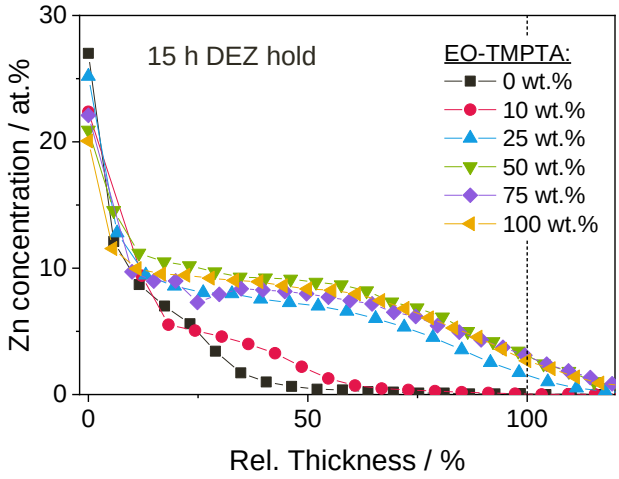

Figure S4: Zn concentration as a function of relative polymer film thickness determined by XPS depth profiling for p(TMPTA-ETPTA) thin films with different compositions after VPI with a 15-hour DEZ hold at 120 ° C.

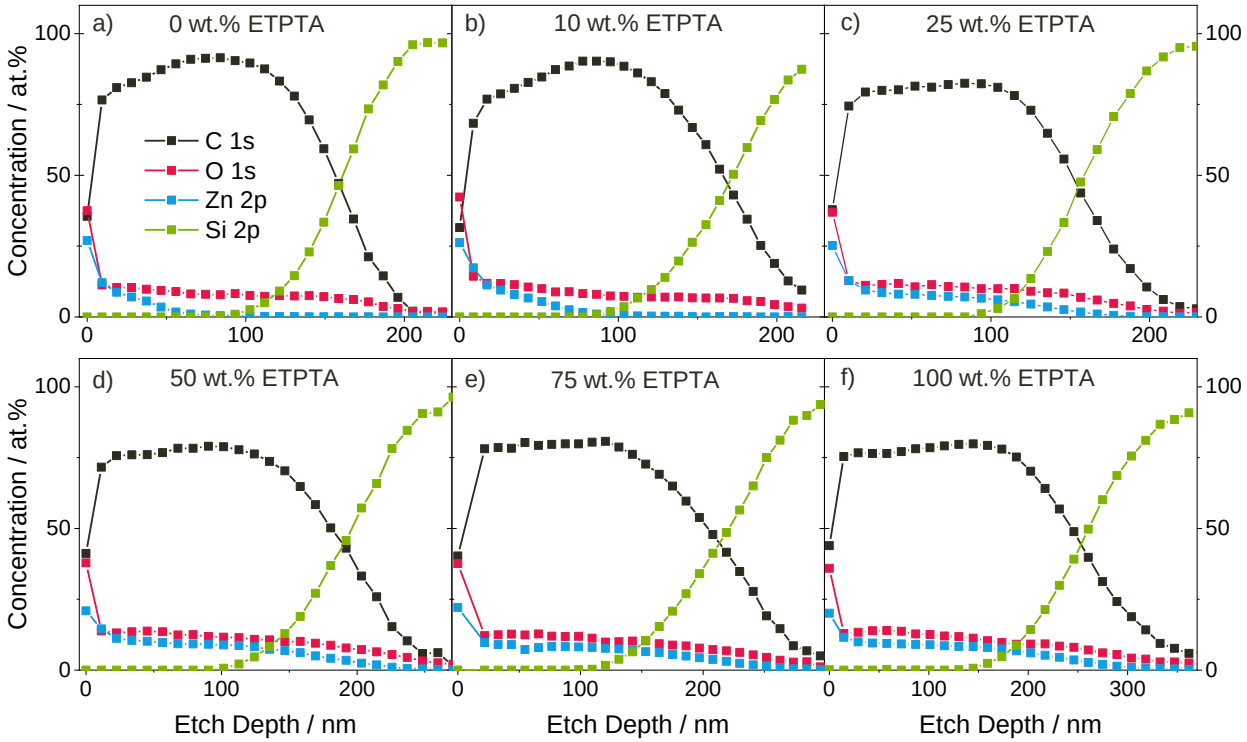

Figure S5: XPS depth profiles of p(TMPTA-ETPTA) films after VPI at 120 ° C with a 15-hour DEZ hold for a) 0 wt.% ETPTA, b) 10 wt.% ETPTA, c) 25 wt.% ETPTA, d) 50 wt.% ETPTA, e) 75 wt.% ETPTA, and f) 100 wt.% ETPTA.

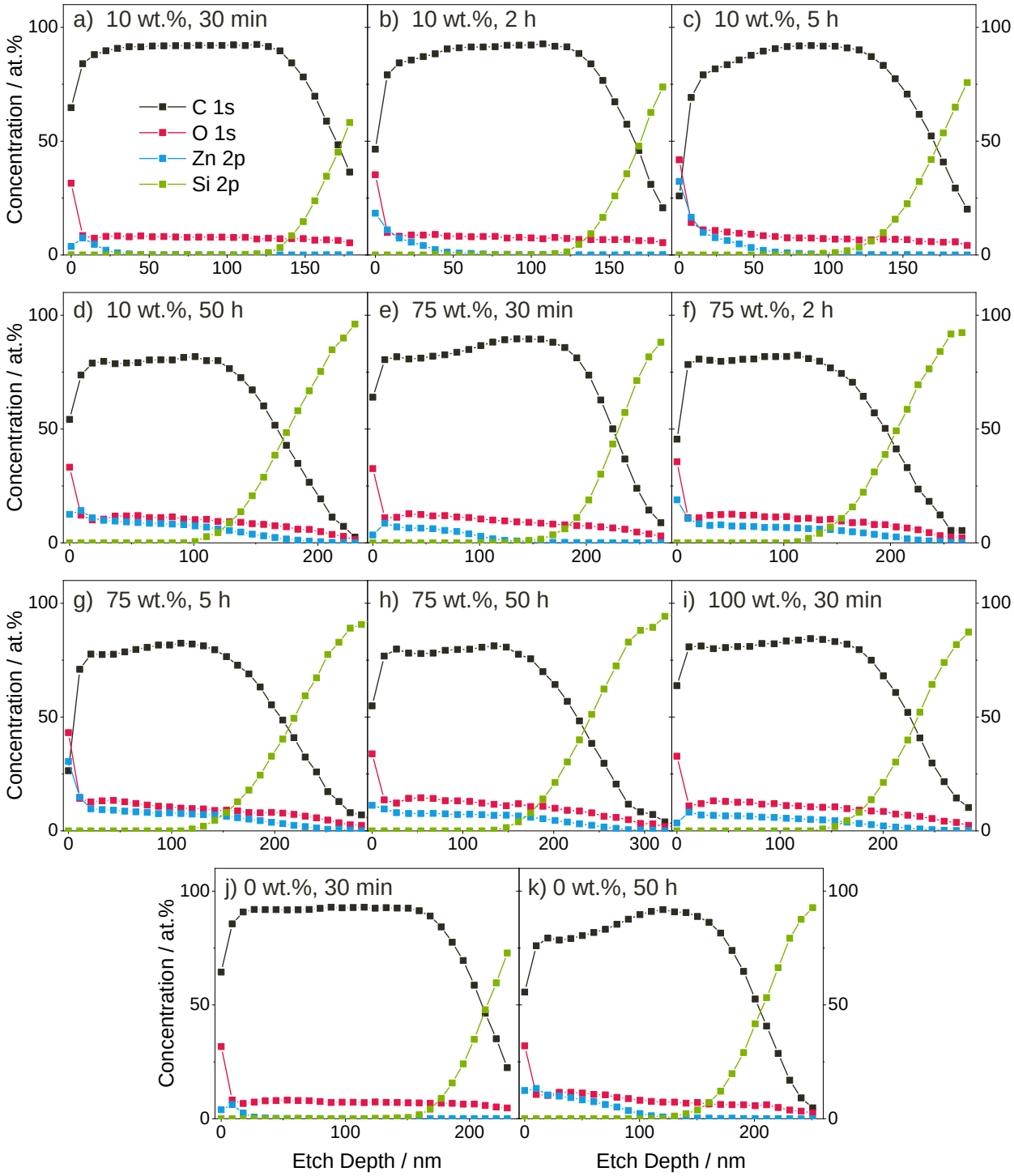

Figure S6: XPS depth profiles of p(TMPTA-ETPTA) films after VPI at 120 ° C for a)-d) 10 wt.% ETPTA and e)-h) 75 wt.% ETPTA and a), e) a 30-minute DEZ hold, b), f) a 2-hour DEZ hold, c), g) a 5-hour DEZ hold, and d), h) a 50-hour DEZ hold. i) shows the depth profile for 100 wt.% ETPTA after a 30-min DEZ hold and j)-k) for 0 wt.% ETPTA and j) a 30-min DEZ hold and k) a 50-hour DEZ hold.

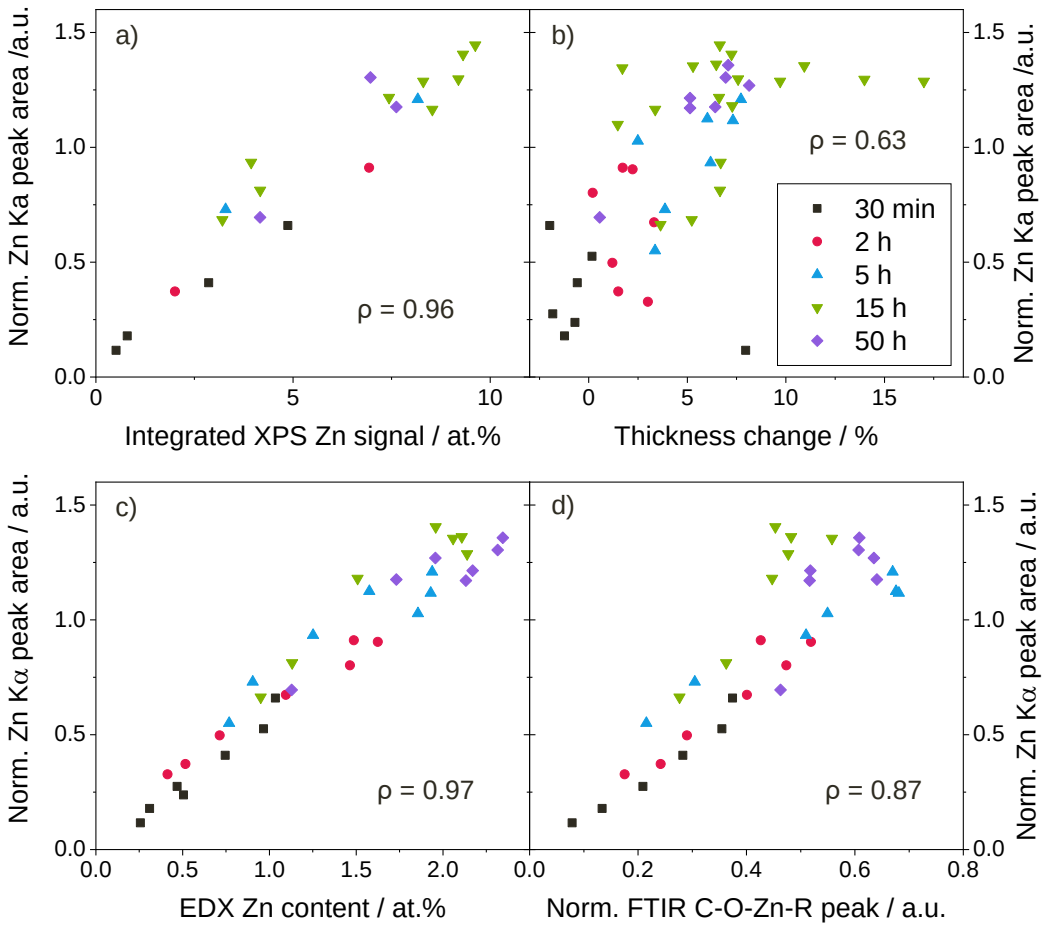

Figure S7: Scatter plots showing the correlation of the Zn loading derived from the thickness-normalized XRF Zn Kα peak area to a) the integrated Zn 2p signal of XPS depth profiling, b) the thickness change upon VPI measured by ellipsometry, c) the atomic Zn concentration determined by EDX, and d) the FTIR intensity of the C-O-Zn-R peak normalized by the intensity of the C=O absorption peak before VPI for copolymer films after VPI at 120 ° C with different DEZ hold times. The Pearson correlation coefficients ρ are given.

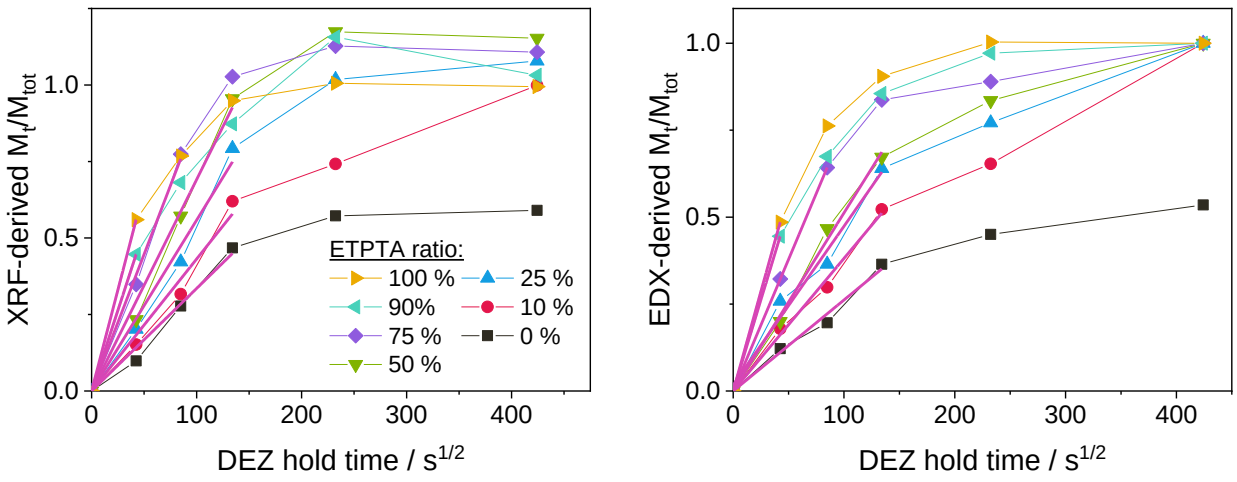

Figure S8: Normalized temporal Zn uptake for p(TMPTA-ETPTA) thin films with different compositions measured by a) XRF and b) EDX. Linear fits used to estimate the diffusion coefficients in **Figure 6** are shown as pink lines.

1) Choice of parameters for reaction-diffusion model

The quantity $C^0_{Polymer}$ was estimated based on the saturated atomic Zn concentration (approximately 8-9 at.%) in the XPS depth profiles. Assuming that each Zn forms a R-Zn-OH bond at a polymer reactive site, with Zn stemming from the precursor and –OH from the co-reaction with water, 8-9 at.% Zn correspond to approximately 2-2.3 Zn atoms/monomer. With a polymer density of roughly 1 g/cm^3, the estimated density of polymer functional groups is 7-8·10^{-3} mol/cm^3. In the model, $C^0_{Polymer} = 10^{-2}\ mol/cm^3$ was used.

It should be noted that XPS might overestimate the atomic Zn concentration due to slower etching of the inorganic compared to the organic species. To obtain a more precise estimate for the density of accessible polymer functional groups, in-situ QCM measurements would be beneficial.

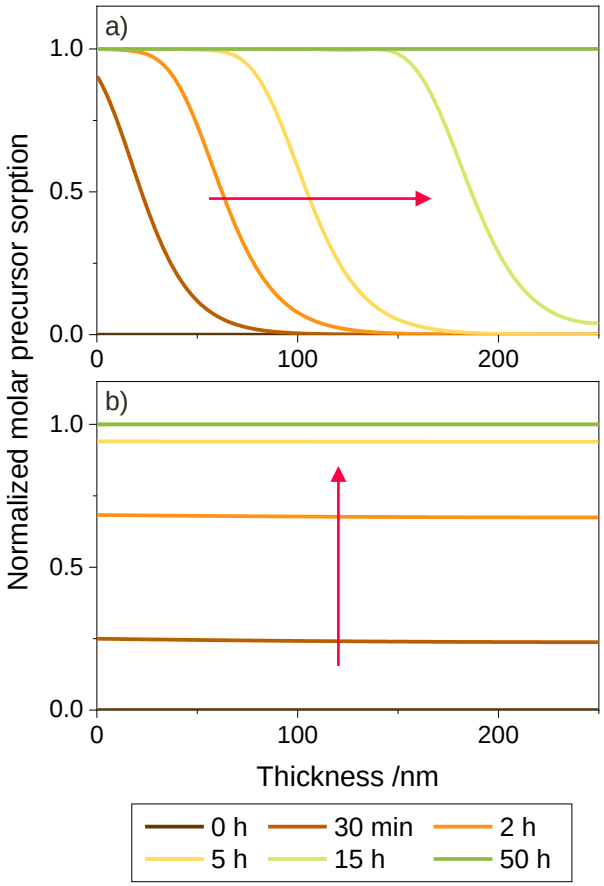

Figure S9: Depth profiles for the normalized concentration of reacted precursor $C_{product}$ at varying precursor exposure times calculated using the reaction-diffusion transport model for a) a diffusion-limited system with high Da = 200, $k = 0.32\ cm^3/(mol \cdot s)$ and $D = 1 \cdot 10^{-14}\ cm^2/s$ and b) a reaction-limited system with low Da = 0.1, $k = 0.04\ cm^3/(mol \cdot s)$ and $D = 5 \cdot 10^{-12}\ cm^2/s$.
Used model parameters are: $K' \cdot C^0_{polymer} = 0.1$, $l = 0.25\ \mu m$, $C^0_{polymer} = 10^{-2}\ mol/cm^3$, $C_s/C^0_{polymer} = 0.4$

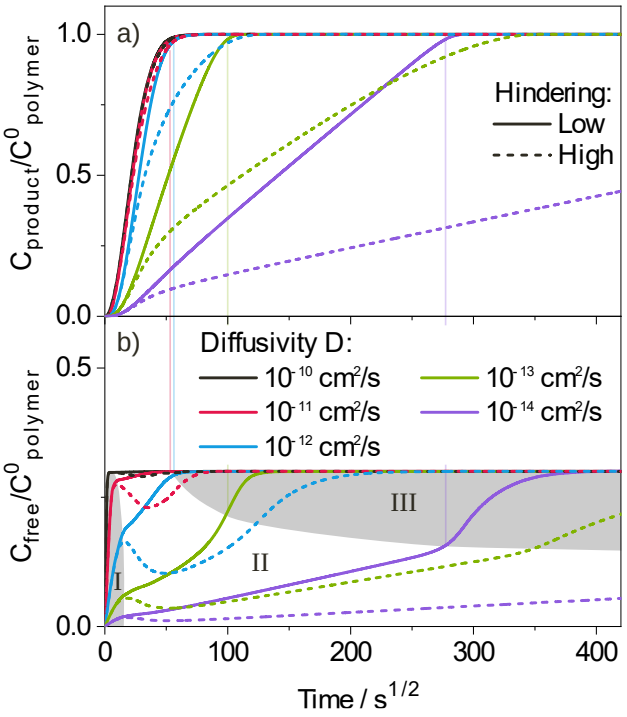

Figure S10: Normalized concentration of a) reacted ($C_{product}$) and b) free (C_{free}) precursor as a function of precursor exposure time calculated using the reaction-diffusion transport model for different diffusivities D with low hindering $K'C^0_{polymer} = 0.1$ (solid line) and high hindering $K'C^0_{polymer} = 4$ (dashed line) . The ratio $C_{product}/C^0_{polymer}$ and $C_{free}/C^0_{polymer}$ represent the amount of reacted and free precursor normalized by the density of reactive polymer sites $C^0_{polymer}$.
Used model parameters are: $k = 0.5\ cm^3/(mol \cdot s)$, $l = 0.2\ \mu m$, $C^0_{polymer} = 10^{-2}\ mol/cm^3$, $C_s/C^0_{polymer} = 0.3$

2) Understanding the calculated temporal uptake curves

For the present system, it is assumed that the reaction rate constant *k*, the density of polymer reactive groups $C^0_{polymer}$, and the sorbed precursor surface concentration C_S are constant, and only investigate the effect of changes in diffusivity *D* and hindering $K'C^0_{polymer}$. **Figure S10** shows the calculated temporal uptake curves for the reacted precursor species ($C_{product}$) and the free precursor (C_{free}). Both quantities are normalized to $C^0_{polymer}$. The formation of $C_{product}$ through chemical reaction depends on C_{free} because the density of free precursors at a given location defines the reaction rate. If $C_{free} = 0$, no reactions can occur. Depending on the rate-limiting process, the increase of $C_{product}$ is either defined by the diffusion rate (i.e diffusion-limited process), which results in a linear increase with the square root of time, by the reaction rate (i.e. reaction-limited process), which results in a linear increase with time, or by a convolution of the two. In varying the diffusivity of the studied systems from 10^{-14} cm^2/s to 10^{-10} cm^2/s, a transition from diffusion-limited to reaction-limited can be observed since the Damköhler number decreases from 200 for $D = 10^{-14}\ cm^2/s$ to 0.02 for $D = 10^{-10}\ cm^2/s$. The infiltration processes depicted in **Figure S10** can be divided into 3 regimes (I, II, III), where the transition between regime I and II corresponds to the on-set of reactions, that is the first formation of $C_{product}$, and the first kink in C_{free}, and the transition between regime II and III corresponds to the point at which reaction saturation ($C_{product}/C^0_{polymer} = 1$) is reached and C_{free} exhibits another change in slope.

During the initial phase of precursor exposure (regime I in **Figure S10b**), pure unhindered diffusion of the precursor takes place, resulting in a linear increase of C_{free} as a function of square root of time. As C_{free} increases, reactions start to take place, resulting in $C_{product} > 0$. A higher diffusivity D results in a steeper slope of C_{free} and hence in an earlier on-set of $C_{product}$ (because more free precursor is present that can react). With the on-set of $C_{product}$, the slope of C_{free} starts to decrease since free precursor is consumed by the reactions.
In a diffusion-limited case ($D \leq 10^{-13}\ cm^2/s$, *Da > 1*), the increase of both C_{free} and $C_{product}$ reaches a steady-slope regime (II) where both quantities increase linearly with the square root of time – because both slopes are determined by Fickian diffusion - until $C_{product}$ reaches saturation (i.e. $C_{product}/C^0_{polymer} = 1$, referred to as reaction saturation). This can be seen best for the case with $D = 10^{-14}\ cm^2/s$ (purple solid line). In general, the slope of both $C_{product}/C^0_{polymer}$ and $C_{free}/C^0_{polymer}$ increases with increasing diffusivity. Once $C_{product}/C^0_{polymer} = 1$, precursor-polymer reactions cease and the slope of C_{free} experiences an increase due to the absence of the reaction sink until $C_{free} = C_S$ (regime III). The state of $C_{free} = C_S$ is referred to as diffusion saturation. Once both $C_{product}/C^0_{polymer} = 1$ and $C_{free} = C_S$, the system has reached diffusion-reaction saturation and does not change anymore during a prolonged precursor exposure.
In a reaction-limited case ($D > 10^{-12}\ cm^2/s$, *Da < 1*), precursor diffusion happens much faster than precursor-polymer reactions. Due to the comparatively fast diffusion, C_{free} reaches values close to or equal C_S during regime I, i.e. before a significant amount of $C_{product}$ is generated. Unless $C_{free} = C_S$ is already reached during regime I, during regime II, C_{free} approaches saturation with a slope reduced by the consumption of free precursor during precursor-polymer reactions, in analogy to the diffusion-limited case.
However, in contrast to the diffusion-limited case described above, the slope of $C_{product}$ is defined by the reaction rate and independent of the precursor diffusivity D. It also increases linearly with time (instead of with the square root of time) until reaction saturation is achieved.

As hindering describes the change in diffusivity of the infiltrated material as a result of precursor-polymer reactions, it only starts to affect the infiltration kinetics once a significant number of precursor molecules have been reacted, i.e. from regime II onwards. If hindering is high, a dip in C_{free} can be observed during regime II in **Figure S10b** before the amount of free precursor starts to increase again. This decrease in C_{free} arises because the consumption of free precursor by reactions is temporarily faster than the re-supply with new free precursor from the surface, since diffusion of the precursor through the reaction-altered polymer is significantly slower than through the pristine polymer. As the availability of free precursor C_{free} is reduced, the slope of $C_{product}$ decreases until a new equilibrium between diffusion and reaction rates is found.

3) The effect of UV polymerization time on DEZ infiltration

It is known that crosslinking density affects the diffusivity of small molecules in polymer networks.[1] A way to vary the density of crosslinking in the p(TMTPA-ETPTA) copolymer system is to vary the UV exposure time during photopolymerization. A previous study[2] showed that with the process conditions described in the experimental section, a 10 min UV exposure is necessary to achieve stable copolymer films. Shorter exposure times lead to a lower degree of vinyl bond conversion and hence a lower crosslinking density, while longer UV times achieve even higher crosslinking with an almost complete conversion of vinyl bonds. The measured Zn loading after VPI with a 15-hour DEZ hold in pTMPTA shows a roughly linear decrease with increasing UV exposure time (see **Figure S11**). XPS depth profiles confirm that Zn penetrates slightly deeper into the polymer for samples with a shorter UV exposure and lower crosslinking density (**Figure S12**). Thermal expansion measurements show that reducing UV exposure time leads to films with a higher thermal expansion coefficient (**Figure S13**). This increase in flexibility can be explained by the lowering of the crosslinking density and can, at least partially, explain the change in infiltration behavior. It should be noted that UV exposure was also shown to cause a certain degree of photooxidation which could generate additional reactive groups for the DEZ precursor, and thus affect zinc loading. A higher density of reactive groups could, on the one hand, enhance inorganic loading because more DEZ reacts with the polymer, or, on the other hand, reduce inorganic loading because it increases hindering and thus slows down diffusion. Further experiments are necessary to properly deconvolute these effects.

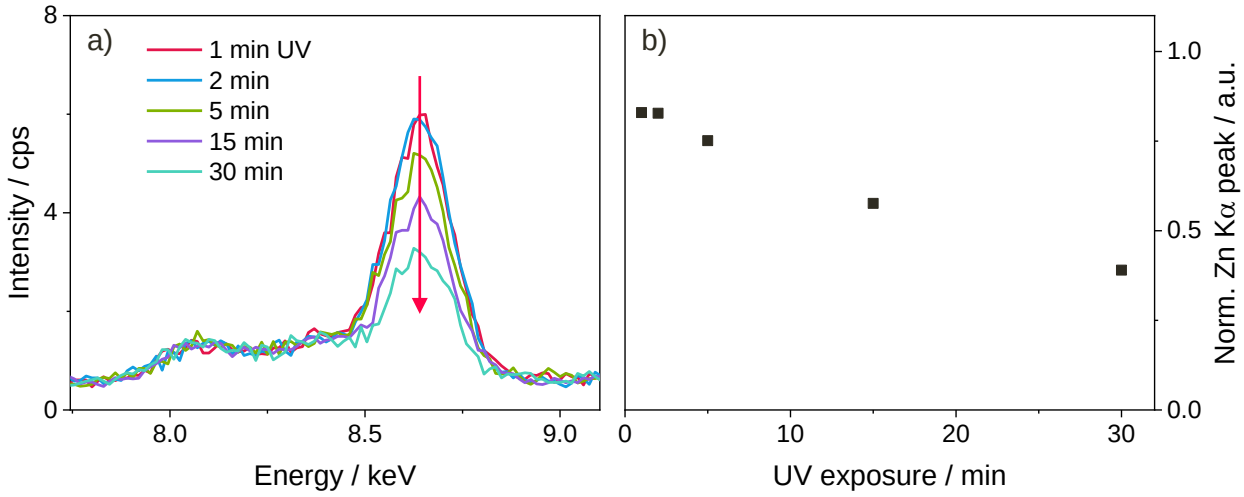

Figure S11: Zinc loading of crosslinked TMPTA for different UV polymerization times after VPI at 120 ° C with a 15-hour DEZ hold. a) XRF Zn Kα peak and b) peak area normalized with respect to the polymer film thickness before VPI as a function of UV exposure time.

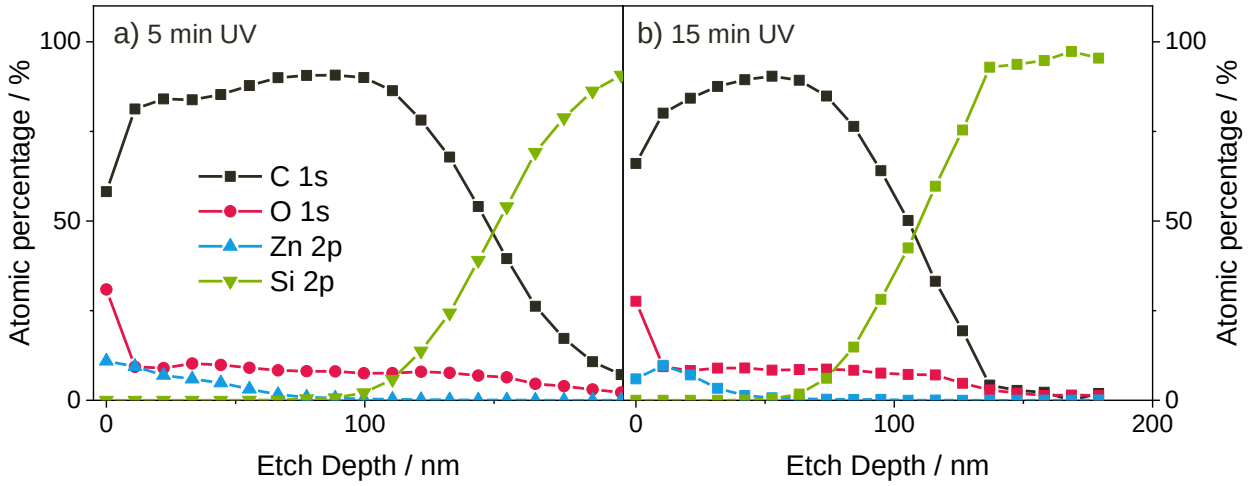

Figure S12: XPS depth profiles of crosslinked TMPTA thin films polymerized under UV for a) 5 min and b) 15 min after VPI at 120° C with a 15-hour DEZ hold.

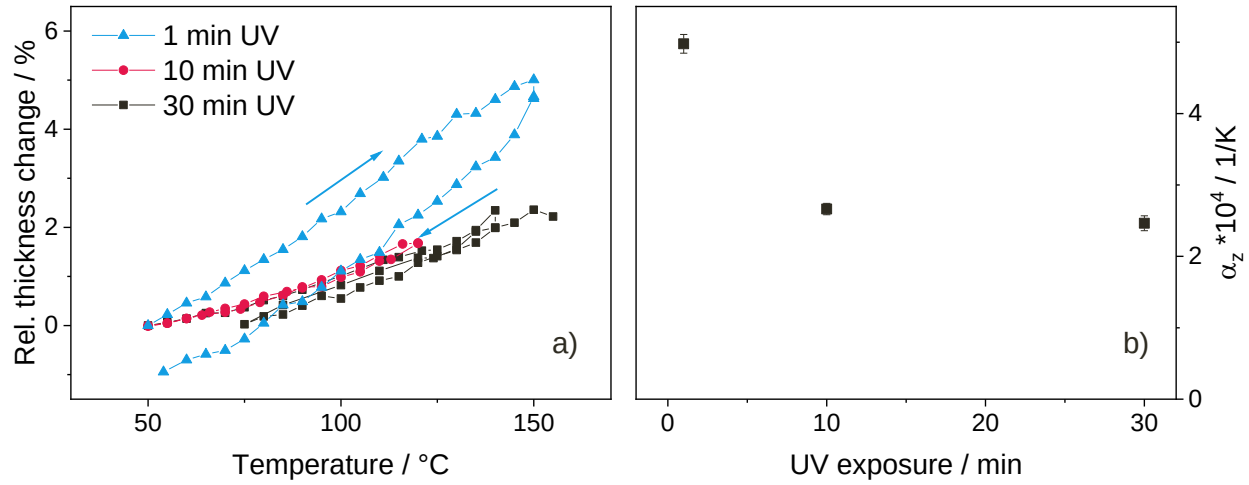

Figure S13: Thermal expansion of crosslinked TMPTA thin films after different UV polymerization times. a) Relative film thickness change measured by ellipsometry and b) linear thermal expansion coefficient in z-direction calculated from the slope in a).

@**Figure S13**: The thermal expansion was measured by a J. A. Woollam Alpha-SE with a wavelength range from 380 to 900 nm at a 70° angle of incidence retrofitted with a custom-built heating stage[3]. Prior to the measurement, the samples were equilibrated at 140 ° C on a hot plate for 1 h. Scans were taken at 5 ° C intervals, and the samples were held ast the maximum temperature for 5 min to check their stability.

References:

[1] S. C. George and S. Thomas, Transport phenomena through polymeric systems, Progress in Polymer Science, 2001, 26, 985–1017.
[2] L. Demelius, L. Zhang, A.M. Coclite, M. Losego, ZnO vapor phase infiltration into photo-patternable polyacrylate networks for the microfabrication of hybrid organic-inorganic structures, Mater. Adv., 2024, 5, 8464-8474.
[3] J. T. Bamford, R. A. Smith, C. Z. Leng, W. R. Gutekunst and M. D. Losego, Measuring the Glass Transition Temperature of Vapor-Phase-Infiltrated AlOx-PS-r-PHEMA Organic–Inorganic Hybrid Thin-Film Materials, Macromolecules, 2021, 54, 6790–6798.